Local-global DVC analyses confirm theoretical predictions for deformation and damage onset in torsion of pantographic metamaterial

Malo Valmalle, Antoine Vintache, Benjamin Smaniotto, F. Gutmann, M. Spagnuolo, A. Ciallella, François Hild

LOCAL-GLOBAL DVC ANALYSES CONFIRM THEORETICAL PREDICTIONS FOR DEFORMATION AND DAMAGE ONSET IN TORSION OF PANTOGRAPHIC METAMATERIAL

M. VALMALLE[1], A. VINTACHE[1], B. SMANIOTTO[1,2], F. GUTMANN[3,4], M. SPAGNUOLO[5,6], A. CIALLELLA[6,7], AND F. HILD[2]

Abstract. Pantographs are a special class of metamaterials that do not obey theories of first gradient continua. In the present work, a pantographic metamaterial was printed and subjected to in situ torsion. The experiment was designed in order to investigate damage onset modalities in large torsional deformations of pantographic mesostructures. To account for the presence of true pivots, multiple point constraints were implemented in the DVC procedure. Local-global DVC was validated thanks to a series of steps accounting for numerous pivots. It was possible to determine the dominant damage mechanism in torsion. Damage was detected thanks to the strain and residual fields. Moreover, important modeling indications were obtained to guide further theoretical and experimental investigations.

1. Introduction

Among mechanical metamaterials, particular interest is payed to those whose mesostructure is made of interacting fibers [1, 2, 3]. In the present study, the mesostructure, also called architecture, was designed to produce macroscopic constitutive equations that were derived *a priori*. The innovative aspect of this description consists precisely in the fact that the metamaterial was considered to be the result of a detailed and precise procedure of synthesis of mesostructure tailored to obtain, after homogenization, the desired mechanical characteristics [4, 5, 6]. Fibrous metamaterials have a further advantage over other ones, namely, they are very easy to manufacture, especially with the recent developments in additive manufacturing techniques, and they exploit the fiber capacity of establishing long range interactions. A "fiber" is a continuous mechanical element in which one dimension prevails over the other two, and for that reason it is easily deformable in bending and much less in tension and shear.

Among the fibrous metamaterials, pantographic architectures are of particular interest as they exploit the bending properties of the fibers in a simple way, based on the manner in which they are connected to one another. A central role lies in the mechanics of the connecting hinges [7, 8, 9]. These hinges exhibit various types of deformation mechanisms, such as torsion and bending due to the relative rotations of the fibers they connect, or shear due to the relative displacements of the fibers. In the mechanical model describing pantographic structures, all these deformation mechanisms need to be taken into account and are represented by means of deformation measures in the postulated strain energy [10, 11, 12, 13]. Using finite element simulations, this energy is employed to calculate the predicted equilibrium configurations and every mechanical quantity of interest by means of minimization.

Date: June 7, 2022.

Key words and phrases. Digital Volume Correlation (DVC), Metamaterial, Multiple point constraints, Torsion test, Uncertainty quantification .

The pantographic structure was designed to make optimal use of the bending properties of the fibers, so that the strain energy describing its macromechanics depends on the second gradient of displacement [14, 15, 16, 17]. It is therefore essential to use a so-called generalized continuum model to describe pantographic structures. It is also important that one measures the deformations of the constituting fibers. For this purpose, the simplest pantographic mesostructure that allows for experimental observations of second gradient effects at the macrolevel consists of a number of long fibers arranged in a rectangular shape (see Figure 1) such that the short side ℓ is at least one third of the long side L. In this way, the fibers linked to the two short edges on which the boundary conditions are prescribed was not stretched but mostly bent. If, instead, one had chosen a square pantographic geometry, the fibers starting from one short edge would be mechanically connected to the opposite (clamped) edge and when conducting, for example, an extension test, these fibers would be forcefully stretched and the elongation energy would prevail over the bending part, thus hiding the second gradient contribution [18, 19, 20, 21].

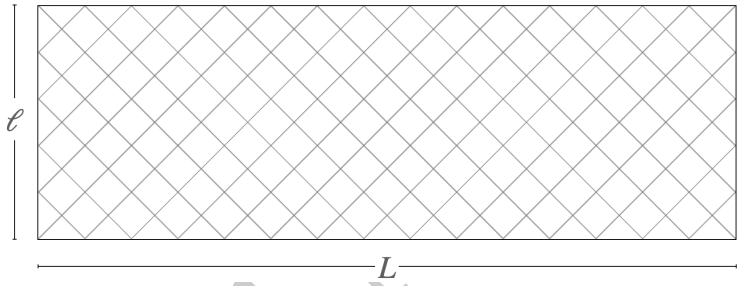

FIGURE 1. Schematic representation of the considered pantographic mesostructure

In order to investigate second gradient effects, and to deactivate some damage mechanisms [22], it was possible to design 3D printing procedures producing perfect hinges, namely, beams interconnecting structural elements allowing for relative fiber rotations in the normal directions with no strain energy. In the present work, the experimental analysis aimed at measuring the deformation in torsion of a pantographic metamaterial with perfect hinges in order to study how the presence of these hinges influences the emergence of Poynting effects [23]. It was observed that pantographic structures with different hinge geometries exhibited direct or reverse Poynting effects [24, 25]. The Poynting effect occurs when a continuum is subjected to torsion and a force is experimentally observed to emerge in the axial direction [23, 26, 27]. This force can be negative or positive, and depending on its sign, there will be a direct or reverse Poynting effect. In pantographic structures this effect was already observed and studied [24], but the effect of perfect hinges was never investigated before neither theoretically nor experimentally.

The *in situ* torsion test was monitored via Digital Image Correlation (DIC) *and* Digital Volume Correlation. As for DIC, there are essentially two types of approaches to measure volumetric displacements, namely, local DVC in which small and independent subvolumes are registered [28, 29] and global (or FE-based) DVC [30] for which the whole region of interest is meshed and correlated in a single analysis. In the present situation, there were different parts that led to independent meshes, each could have been registered alone. However, additional constraints were implemented to couple them by accounting for the presence of hinges. Consequently, this type of procedure is referred to as local-global DVC.

Please cite this document as: M. Valmalle, A. Vintache, B. Smaniotto, F. Gutmann, M. Spagnuolo, A. Ciallella, F. Hild, "Local-global DVC analyses confirm theoretical predictions for deformation and damage onset in torsion of pantographic metamaterial", *Mechanics of Materials* (2022), doi:https://doi.org/10.1016/j.mechmat.2022.104379.

The main feature of pantographic mesostructures lies in the possibility of large relative rotations and displacements of very close structural elements. Therefore, the aforementioned DVC analysis was essential in order to experimentally check the designed properties of such metamaterials. In particular, one has to verify that the largest part of strain energy is concentrated in elastic hinges or, when perfect hinges are present, in hinge deformation and in fiber bending.

The outline of the paper is as follows. First, the *in situ* torsion experiment is presented. Then, the different steps of the local-global DVC approach are introduced. The measured displacement fields, corresponding strain and residuals fields are analyzed to detect damage. In the last section, the experimental results obtained via DVC are compared to theoretical analyses based upon the model proposed by Giorgio et al. [31]. This constitutive law is purely elastic. However, it allows for the prediction of damage initiation if a yield criterion based on a strain energy threshold is introduced.

2. In Situ Torsion test

The pantographic metamaterial studied hereafter was fabricated by additive manufacturing via Selective Laser Melting (SLM) on an EOS M 100 machine with a 200-W laser unit (YLR,Äëseries, CW,Äëlaser, wavelength: 1070 nm) in 20 µm layers. It was printed in a 45° orientation to the build plate to reduce acute angles. An argon-based inert gas atmosphere with $O_2 < 0.1\%$ was selected to prevent oxidation from occurring during the fabrication process. The bulk material was Ti-6Al-4V (or Ti64), namely, an alpha-beta titanium alloy. The dimensions of the sample were chosen such that one side was three times longer than the other one. More precisely, the pantographic structure (Figure 2(a)) had the shape of a rectangle of sides 30.3 mm and 90 mm, and the external width was equal to 8.4 mm. The beams had a square section of 2.2×2.2 mm in area, and the connections were pivoting links whose inner diameter was 0.8 mm, outer diameter 2 mm, and length 7 mm (see Figure 2(b)). The clearance in each pivoting link was equal to 250 µm on the diameter. These values are nominal and were used to design the pantograph in the CAD modeler. The resulting CAD file was then used to print the sample.

Contrary to a previous study [25], each link between the two families of beams had a pivot shaft with a smaller inner diameter so that it was stopped along its longitudinal direction (Figure 2(c-d)). An average clearance of the order of 320 µm on the diameter was estimated on the reconstructed volume. This value is greater than the nominal level (*i.e.,* 250 µm). The quality of the printed sample is shown in Figure 2(c) for a high resolution scan (*i.e.,* 6.5 µm / vx) of one pivoting link. The corresponding section shows that the pivots were successfully printed with the selected resolution (*i.e.,* 20 µm layers).

Please cite this document as: M. Valmalle, A. Vintache, B. Smaniotto, F. Gutmann, M. Spagnuolo, A. Ciallella, F. Hild, "Local-global DVC analyses confirm theoretical predictions for deformation and damage onset in torsion of pantographic metamaterial", *Mechanics of Materials* (2022), doi:https://doi.org/10.1016/j.mechmat.2022.104379.

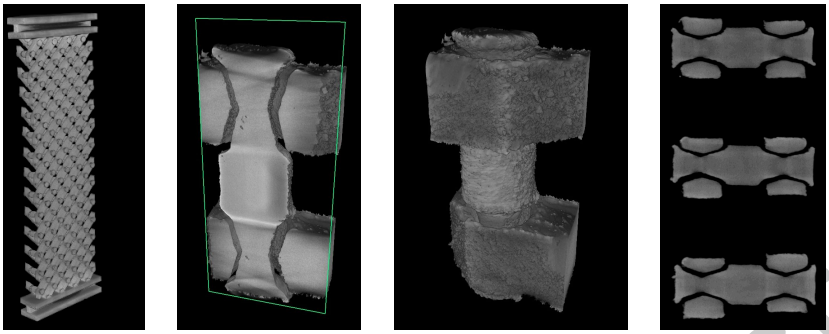

(a) (b) (c) (d)

FIGURE 2. (a) Printed metamaterial. (b) Low resolution (*i.e.,* 66 µm / vx) section showing three pivoting links. (c) High resolution (*i.e.,* 6.5 µm / vx) 3D rendering of one link, and (d) corresponding section. The beam section is equal to 2.2×2.2 mm^2

The torsion test was monitored using micro-computed tomography [32]. Such imaging technique is non-intrusive and provides 3D images of the sample tested in situ [33]. Special 3D printed grips made of ABS were used to enable the total height of the sample to be imaged (*i.e.,* they were virtually transparent to X-rays). Nylon screws were used to fix them on the bottom and top platens of the testing machine (Figure 3(a)). The torsion torque is the response to the twist angle prescribed by the two rotational actuators of the in situ testing machine. The test was conducted up to failure (Figure 3).

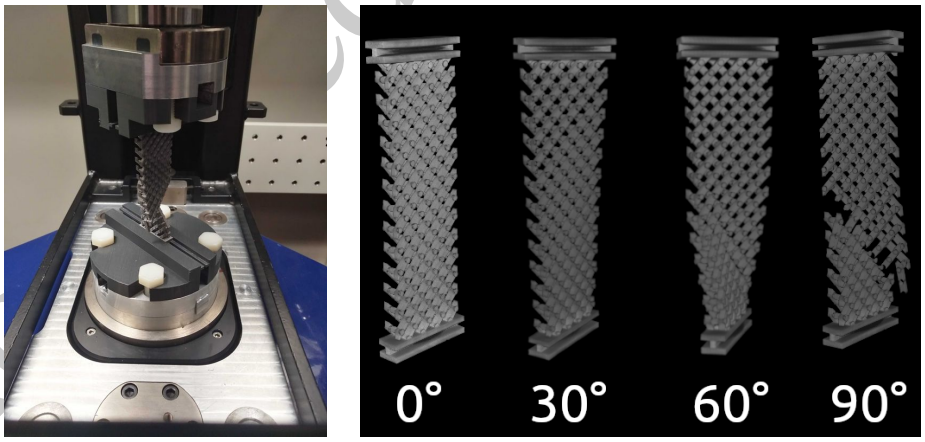

(a) (b)

FIGURE 3. (a) Broken sample in the in situ testing machine. (b) 3D renderings of the reference configuration (0°) and deformed configurations with three different angular amplitudes

Five scans were performed, namely, two in the reference configuration for uncertainty quantification, and three in the deformed configurations. The last one was post-failure.

Please cite this document as: M. Valmalle, A. Vintache, B. Smaniotto, F. Gutmann, M. Spagnuolo, A. Ciallella, F. Hild, "Local-global DVC analyses confirm theoretical predictions for deformation and damage onset in torsion of pantographic metamaterial", *Mechanics of Materials* (2022), doi:https://doi.org/10.1016/j.mechmat.2022.104379.

Series of 700 radiographs per scan (*i.e.,* sinograms) were acquired to reconstruct 3D images of the sample (Figure 3(b)). The hardware parameters of the in situ setup are gathered in Table 1. Once cropped, the reconstructed volumes covered $49.6 \times 50.0 \times 93.6$ mm^3 with a 66 µm / vx resolution.

Table 1. DVC hardware parameters

Tomograph	North Star Imaging X50+
X-ray source	XRayWorX XWT-240-CT
Target / Anode	W (reflection mode)
Filter	Al (1.5 mm)
Voltage	150 kV
Current	100 µA
Focal spot size	5 µm
Tube to detector	500 mm
Tube to object	215 mm
Detector	Dexela 2923
Definition	1536×1944 pixels (2×2 binning)
Number of projections	700
Angular amplitude	360°
Frame average	10 per projection
Frame rate	8 fps
Acquisition duration	23 min 28 s
Reconstruction algorithm	filtered back-projection
Gray Levels amplitude	8 bits
Volume size	$751 \times 757 \times 1418$ voxels (after crop)
Field of view	$49.6 \times 50.0 \times 93.6$ mm^3 (after crop)
Image scale	66 µm/voxel

The levels of torque and axial force were continuously recorded during the deformation process (Figure 4). Even though only one scan was performed in the elastic range, the gathered data were sufficient to calibrate the numerical model used herein. The initial plateau in both torque and normal force plots are most likely justified with the concurrence of two phenomena: (i) taking up the clearance in the hinges, and (ii) the immediate activation of second gradient bending strain energy due to the absence of torsional elastic hinges. This last point will need a further experimental analysis The elastic range seems to be mainly linear in both plots, exactly as predicted by the model presented in last section. Damage before failure shows the characteristic pattern presented in pantographic mesostructures, namely, the local failure of one structural element activated the deformation of neighboring joints, thereby increasing the resistance of the whole structure. This effect is more pronounced in the induced normal force than in the reaction torque. It is noteworthy that the induced normal force is mainly determined by the axial stiffness of the fiber array. Instead, the torque is associated with the stiffnesses relative to fiber bending and torsion, hinge elongation, shear and bending. In order to get correct predictions via numerical simulations, it is necessary to calibrate such stiffnesses taking into account their role in the Poynting effect.

Please cite this document as: M. Valmalle, A. Vintache, B. Smaniotto, F. Gutmann, M. Spagnuolo, A. Ciallella, F. Hild, "Local-global DVC analyses confirm theoretical predictions for deformation and damage onset in torsion of pantographic metamaterial", *Mechanics of Materials* (2022), doi:https://doi.org/10.1016/j.mechmat.2022.104379.

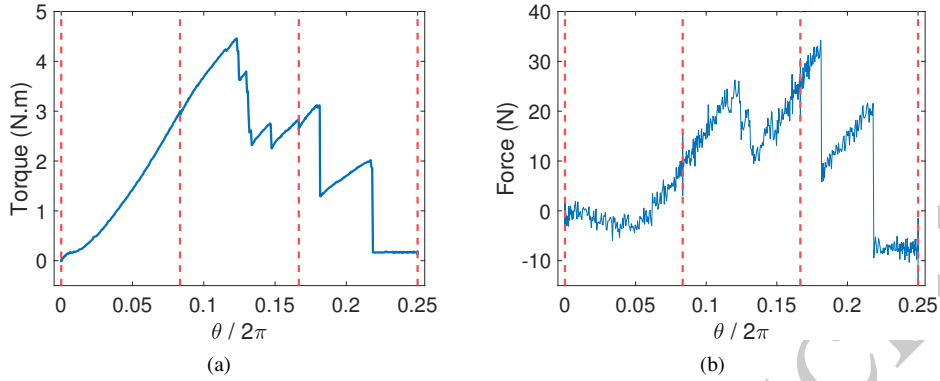

FIGURE 4. Torque (a) and induced normal force (b) of the in situ torsion test. The red dashed lines depict scan acquisitions

3. Different DVC Steps

Only two scans of deformed configurations prior to fracture were available (Figure 3(b)). Given the large angular amplitudes between each acquisition, the DVC analyses had to be tailored to the present case by the following steps.

3.1. Regularized DVC.

The DVC analyses reported hereafter were FE-based [30, 34]. Consequently, the sought displacement field reads

$$\mathbf{u}(\mathbf{x}, \{\boldsymbol{\upsilon}\}) = \sum_i \upsilon_i \mathbf{N}_i(\mathbf{x}) \tag{1}$$

where $\mathbf{N}_i(\mathbf{x})$ are the vectorial shape function associated with the nodal displacement υ_i. The latter ones, which are gathered in the column vector $\{\boldsymbol{\upsilon}\}$, are the unknowns to be measured. They were determined by minimizing the sum of squared differences over the considered region of interest (ROI)

$$\{\boldsymbol{\upsilon}\}_{\text{meas}} = \arg\min_{\{\boldsymbol{\upsilon}\}} \Phi_c^2(\{\boldsymbol{\upsilon}\}) \tag{2}$$

with

$$\Phi_c^2(\{\boldsymbol{\upsilon}\}) = \sum_{\mathbf{x}\in\text{ROI}} \rho^2(\mathbf{x}, \{\boldsymbol{\upsilon}\}) \tag{3}$$

where ρ denotes the gray level residual computed for every voxel belonging to the ROI

$$\rho(\mathbf{x}, \{\boldsymbol{\upsilon}\}) = f(\mathbf{x}) - g(\mathbf{x} + \mathbf{u}(\mathbf{x}, \{\boldsymbol{\upsilon}\})) \tag{4}$$

Since the mesoscale mesh was very fine (*i.e.,* 5-vx elements were utilized, see Figure 6) and not many printing defects were observed (Figure 2(d)), DVC had to be regularized [35]. In the present case, Hencky-elasticity was considered to deal with large transformations [36, 25]. A penalty term was added to the global residual Φ_c^2, which refers to the equilibrium gap [37]

$$\Phi_m^2(\{\boldsymbol{\upsilon}\}) = \{\boldsymbol{\upsilon}\}^\top [\mathbf{K}]^\top [\mathbf{K}] \{\boldsymbol{\upsilon}\} \tag{5}$$

such that the weighted sum is minimized to determine the nodal displacements via regularized DVC

$$\{\boldsymbol{\upsilon}\}_{\text{meas}} = \arg\min_{\{\boldsymbol{\upsilon}\}} \left(\Phi_c^2(\{\boldsymbol{\upsilon}\}) + w_m \Phi_m^2(\{\partial\boldsymbol{\upsilon}\}) \right) \tag{6}$$

where $\{\partial\boldsymbol{\upsilon}\}$ denotes the column vector of incremental displacements from one analysis to the next, $[\mathbf{K}]$ the rectangular stiffness matrix associated with bulk and free surface nodes.

Please cite this document as: M. Valmalle, A. Vintache, B. Smaniotto, F. Gutmann, M. Spagnuolo, A. Ciallella, F. Hild, "Local-global DVC analyses confirm theoretical predictions for deformation and damage onset in torsion of pantographic metamaterial", *Mechanics of Materials* (2022), doi:https://doi.org/10.1016/j.mechmat.2022.104379.

The regularization weight is proportional to a length, referred to as regularization length ℓ_m, raised to the power 4 [35].

3.2. **Mesh in the reference configuration.** FE-based DVC [30] was used in the present analyses. Such approach required an FE mesh to be constructed. In the present case, the starting point was the CAD model of the to-be-printed pantograph. This initial information corresponds to the nominal configuration of the digital twin (Figure 5). The Catia modeler allows meshes to be created (*i.e.,* four-noded (T4) tetrahedra). Because of small printing errors, the (experimental) reference configuration did not coincide with the digital twin. Therefore, a backtracking procedure [25] was needed to fit the digital twin onto the printed geometry. This procedure consists in registering the reference configuration with the voxelized digital twin, which was constructed from the STL model of the nominal configuration (also generated with the CAD modeler). With the STL file, a ray tracing algorithm [38] was used to create the voxelized twin.

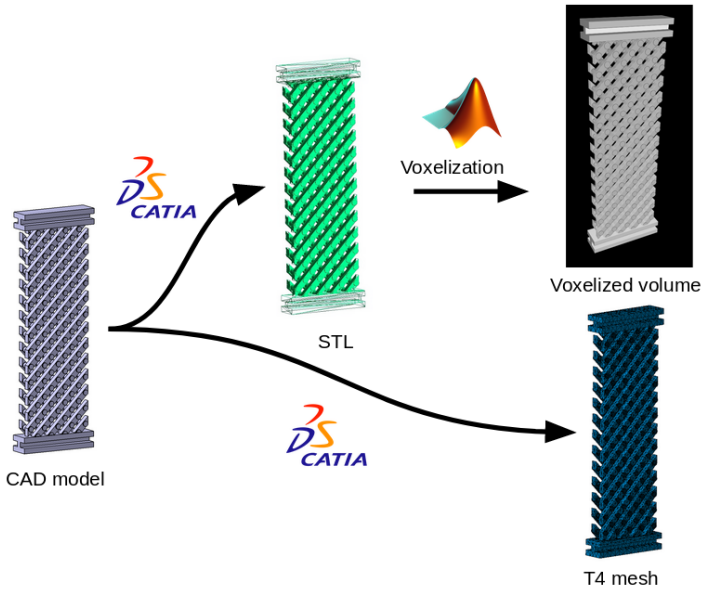

FIGURE 5. Digital twins of the nominal configuration of the studied pantograph

Figure 6 shows the mesh in the nominal configuration. All pivoting links were explicitly meshed. In particular, each shaft was discretized with fine details. Conversely, the geometric details of each beam close to the connections were not as fine. This choice resulted from compromises between mesh fineness, voxel resolution and size of the DVC problem. The mesh contained 67,067 nodes and 209,608 T4 elements whose mean size (measured as the cube root of the average elementary volume) was 5 vx.

Please cite this document as: M. Valmalle, A. Vintache, B. Smaniotto, F. Gutmann, M. Spagnuolo, A. Ciallella, F. Hild, "Local-global DVC analyses confirm theoretical predictions for deformation and damage onset in torsion of pantographic metamaterial", *Mechanics of Materials* (2022), doi:https://doi.org/10.1016/j.mechmat.2022.104379.

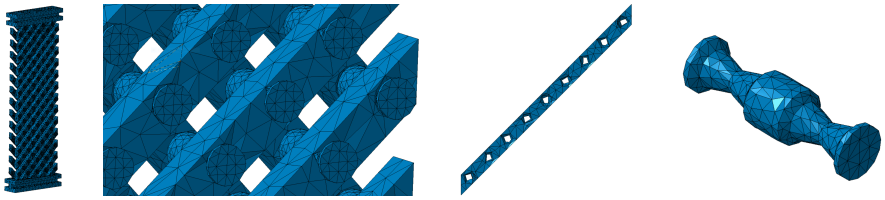

FIGURE 6. (a) Mesh in the nominal configuration. Details showing pivoting links (b), one beam (c), and one shaft (d)

As the printed sample was slightly warped by the printing process, a preliminary DVC analysis was conducted between the voxelized twin and the printed shape to backtrack the mesh that was constructed on the nominal geometry (Figure 7). An auxiliary mesh encompassing the volume in the reference configuration was considered and regularized DVC [35] was run. since virtually no contrast existed within the printed solid phase (Figure 2).

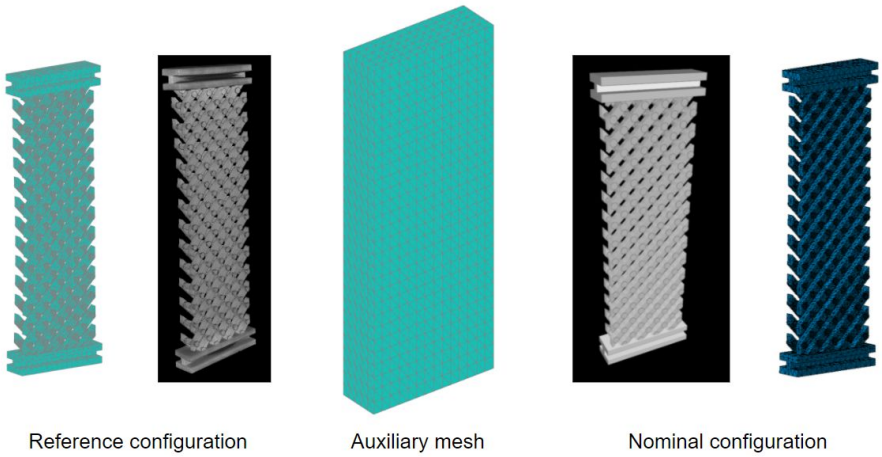

FIGURE 7. Reference (printed) configuration to be registered with the nominal configuration via regularized DVC using an auxiliary mesh encompassing the reference configuration

Figure 8 shows the displacement field that had to be applied between the printed and nominal configurations. The rigid motions were taken out since they were due to the fact that the reconstruction frame and the digital twin were not perfectly aligned. The longitudinal (*i.e.,* along z) displacement field indicates that the reference configuration was shorter than the nominal configuration. This shortening was due to gravity that led to contacts in the hinges as opposed to the nominal configuration for which no contact occurred. The transverse (*i.e.,* along x) displacement field shows that the sample had an S-shape in the $x-z$ plane. Last, the out-of-plane (*i.e.,* along y) displacement field reveals that there was an additional curvature of the sample.

Please cite this document as: M. Valmalle, A. Vintache, B. Smaniotto, F. Gutmann, M. Spagnuolo, A. Ciallella, F. Hild, "Local-global DVC analyses confirm theoretical predictions for deformation and damage onset in torsion of pantographic metamaterial", *Mechanics of Materials* (2022), doi:https://doi.org/10.1016/j.mechmat.2022.104379.

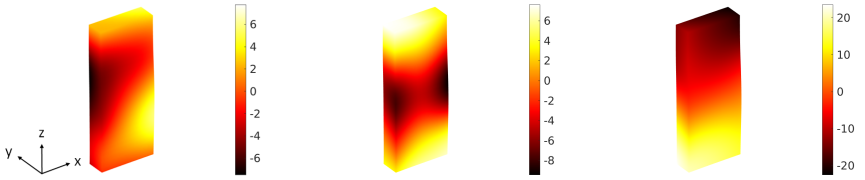

(a) (b) (c)

FIGURE 8. Displacement fields in x (a), y (b) and z (c) directions for the backtracking procedure. The fields are shown on the deformed configuration and expressed in voxels

In Figure 9, sections of the gray level residuals are shown for two planes containing a family of beams. Overall, the registration was successful since each shaft and beam was repositioned. There are still some small mismatches in particular of the back section due to small printing errors. The streaks that appear in the background are due to tomography artifacts [39].

(a) (b)

FIGURE 9. Sections of gray level residuals for the front (a) and back (b) families of beams

3.3. **Accounting for pivoting joints.** Up to this point, the presence of the pivoting links was not accounted for when running DVC analyses. Therefore, the corresponding surfaces on the shafts and beams may interpenetrate. To avoid such phenomenon, new constraints had to prescribed to the minimization scheme. Such situations were already encountered in DIC [40, 41]. Constraint conditions are commonly applied in FE analyses [42]. Three routes are generally followed. First, Lagrange multipliers can be used and these additional unknowns increase the number of equations of the linear system. They were applied for prescribing exactly zero displacement jumps at hinges of pantographic metamaterials [41]. Second, multiple point constraints with the linear transformation method enable the number of unknowns to be reduced via master/slave considerations [40]. Last, penalty methods conserve the number of system variables but may lead to ill-conditioned sets of equations [43]. Given the fact that a penalty term was already introduced in the present case (Equation (6)),

Please cite this document as: M. Valmalle, A. Vintache, B. Smaniotto, F. Gutmann, M. Spagnuolo, A. Ciallella, F. Hild, "Local-global DVC analyses confirm theoretical predictions for deformation and damage onset in torsion of pantographic metamaterial", *Mechanics of Materials* (2022), doi:https://doi.org/10.1016/j.mechmat.2022.104379.

it was decided to add another term to account for the pivoting links

$$\Phi_p^2(\{\boldsymbol{v}\}) = \sum_j (kK_{\max}[\![\boldsymbol{v}_j]\!])^2 \tag{7}$$

such that

$$\{\boldsymbol{v}\}_{\text{meas}} = \arg\min_{\{\boldsymbol{v}\}} \left(\Phi_c^2(\{\boldsymbol{v}\}) + w_m\Phi_m^2(\{\partial\boldsymbol{v}\}) + w_m\Phi_p^2(\{\partial\boldsymbol{v}\})\right) \tag{8}$$

where $K_{\max}$ denotes the maximum diagonal term of the stiffness matrix $[\mathbf{K}]$, $[\![\boldsymbol{v}_j]\!]$ the displacement jump of the j-th pivoting link, and k an additional weight to tailor this last penalization wrt. to the bulk regularization. With this setting, additional non-zero terms were created in the global stiffness matrix $[\mathbf{K}]$. This observation explains the reason for making the two penalty terms of identical dimensions by introducing $K_{\max}$. In practice, the nodes corresponding to each neck of the connecting links were sought (Figure 10). Then, the difference in average displacement of the inner nodes (belonging to the beams) and outer nodes (belonging to the shafts) correspond to the displacement jump $[\![\boldsymbol{v}_j]\!]$ to be penalized. Once the nodes of the 234 links were found (Figure 10), additional terms were added to the stiffness matrix. It is worth mentioning that the rotations were not penalized.

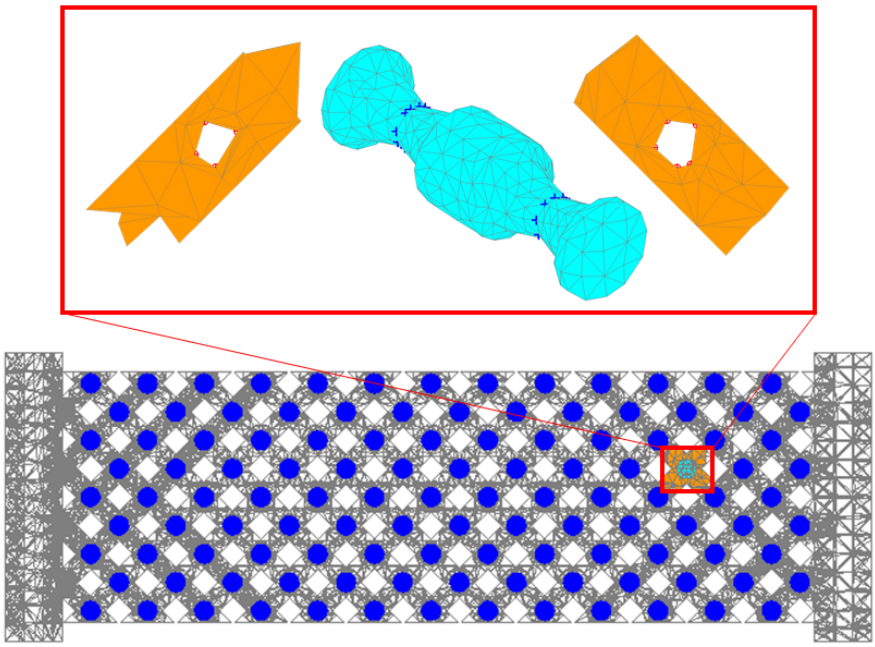

FIGURE 10. Identification of pivoting links (blue) in the FE mesh. The nodes marked with red and blue crosses (see inset) were considered to compute the displacement jump of each pivoting link

The reconstructed volumes were registered using the Correli 3.0 framework [44] in which the two regularization terms were implemented (Table 2). The uncertainty quantification to evaluate the noise floor levels was based on the two scans of the reference configuration. A DVC analysis was run with the backtracked mesh (Figures 7) for a regularization length ℓ_r equal to 30 vx. Rigid body motions were subtracted from the measured displacement

Please cite this document as: M. Valmalle, A. Vintache, B. Smaniotto, F. Gutmann, M. Spagnuolo, A. Ciallella, F. Hild, "Local-global DVC analyses confirm theoretical predictions for deformation and damage onset in torsion of pantographic metamaterial", *Mechanics of Materials* (2022), doi:https://doi.org/10.1016/j.mechmat.2022.104379.

fields, the standard deviations of each nodal displacement component was estimated and is reported in Table 2. Rather low levels are observed thanks to the regularization strategy used herein. The standard uncertainty of any displacement jump component was equal to 0.04 vx (Figure 11).

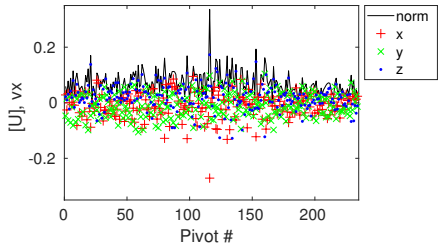

FIGURE 11. Displacement jumps in the 234 pivots for the analysis of the repeated scan

Two strain components are to be reported in the sequel, namely, the maximum principal strain ϵ_1 and the equivalent von Mises strain ϵ_{eq}. Their corresponding uncertainties were virtually identical and respectively equal to 2.7×10^{-3} and 3×10^{-3}. These levels show that elastic strains cannot be measured accurately. Conversely, plastic strains can be quantified for levels greater than 10^{-2}.

TABLE 2. DVC analysis parameters

DIC software	Correli 3.0 [44]
Image filtering	none
Element length (mean)	5 voxels
Shape functions	linear (T4)
Mesh	see Figure 6
Matching criterion	penalized sum of squared differences (7)
Regularization length and ratio	$\ell_m = 30$ vx, $k = 1$
Interpolant	cubic
Displacement noise floor	0.06 / 0.04 / 0.06 vx
Displacement jump noise floor	0.04 vx (same for all directions, Figure 11)
Strain noise floor	3×10^{-3}

3.4. **Initialization.** Due to the large deformations between each angular amplitude for which scans were acquired, the DVC calculations had to be initialized. A digital image correlation algorithm was used on each nodal plane of a coarse dogbone mesh encompassing the sample (Figure 12) seeking in-plane rigid body motions (*i.e.,* assuming that there was no Poynting effect [23, 26, 27]). Because the same angular amplitudes were applied to the top and bottom grips, the middle section of the pantograph was expected to be essentially motionless. Accordingly, the DIC calculations were run from the middle nodal plane along the top and the bottom separately, using the rigid body of the previous nodal plane to initialize the next DIC calculation. The displacement field found at this stage was then used as initialization for first DVC calculations (Figure 6), which converged in 13 and 47 iterations for a convergence criterion of 10^{-3} vx. In the present cases, no incremental evaluations were needed and direct registrations could be performed.

Please cite this document as: M. Valmalle, A. Vintache, B. Smaniotto, F. Gutmann, M. Spagnuolo, A. Ciallella, F. Hild, "Local-global DVC analyses confirm theoretical predictions for deformation and damage onset in torsion of pantographic metamaterial", *Mechanics of Materials* (2022), doi:https://doi.org/10.1016/j.mechmat.2022.104379.

Figure 12 shows the measured displacement fields. It is worth noting that very large amplitudes occurred for the out-of-plane (y) direction. Had the DVC analyses not been initialized, the convergence would have been very slow if possible. It is interesting to note that significant longitudinal displacements are observed in addition to the normal force reported in Figure 4(b). Both data underline a macroscopic Poynting effect that was already observed for different pantographic geometries [24, 25].

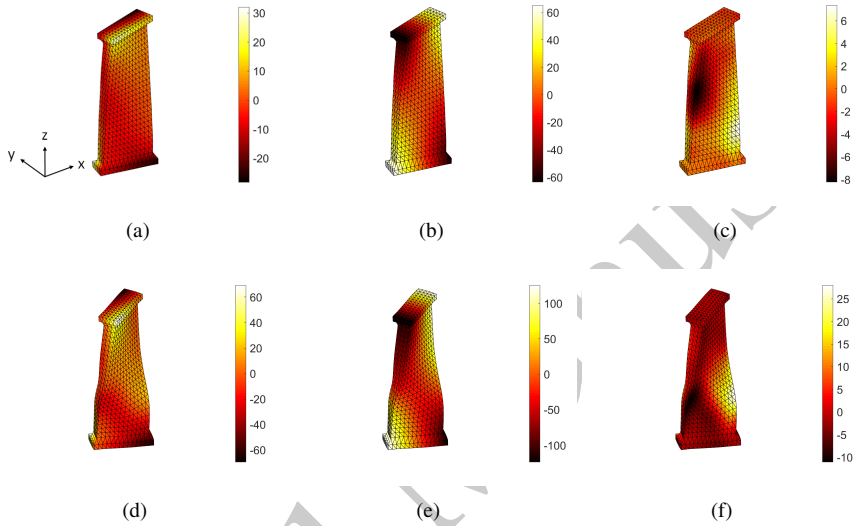

FIGURE 12. Displacement fields in x (a,d), y (b,e) and z (c,f) directions for the first (a,b,c) and second (d,e,f) deformed scans. The fields are shown on the deformed configurations and expressed in voxels

4. ANALYSIS OF THE RESULTS

The displacements measured on the first macroscopic mesh (Figure 12) were used to initialize the DVC analyses utilizing the backtracked mesh (Figure 7). The DVC calculations were stopped when the norm of displacement corrections were less than 5×10^{-2} vx and 10^{-1} vx for the two analyzed scans.

4.1. Registration and Equilibrium Residual Fields.

Before discussing any result, the first field to check is the gray level (registration) residuals ρ (see Equation (4)). This field is reported for the front and back faces in Figure 13. For the first scan, after initialization, the root mean square (RMS) residual was equal to 13.7 gray levels and after the DVC calculation it reached 8.9 gray levels, namely, less than two times that of the registration for uncertainty quantification (*i.e.,* 4.6 gray levels). Consequently, the DVC result was deemed trustworthy. Different "bands" are observed on the two families of beams (Figure 13(a,b)). In particular, high values are observed near the heads of some shafts, which indicate locations were the joints experienced larger displacements than allowed by the regularization.

For the second scan, the RMS residual was equal to 37.3 gray levels after initialization. Following the DVC calculation, the RMS residual reached 17.6 gray levels. Compared to the first scan, this new level almost doubled. This results shows that the measured kinematics was less consistent with the experiment (*i.e.,* due to the development of damage). There are

Please cite this document as: M. Valmalle, A. Vintache, B. Smaniotto, F. Gutmann, M. Spagnuolo, A. Ciallella, F. Hild, "Local-global DVC analyses confirm theoretical predictions for deformation and damage onset in torsion of pantographic metamaterial", *Mechanics of Materials* (2022), doi:https://doi.org/10.1016/j.mechmat.2022.104379.

various zones of very high residuals in Figure 13(c,d), which correspond to damaged areas in which the connecting links were broken. It is interesting to note that these new "bands" were not those with the highest residuals in the first scan (Figure 13(a,b)).

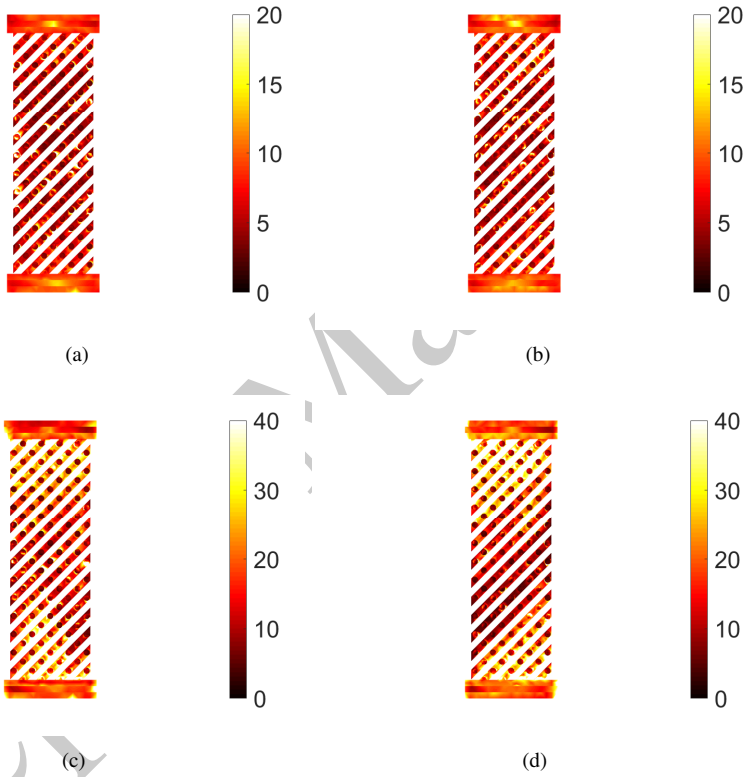

FIGURE 13. Gray level residual fields on the front (a,c) and rear (b,d) surfaces for the first (a,b) and second (c,d) deformed scans

The second field to observe is the norm of the nodal equilibrium residual $\{\boldsymbol{f}_{res}\}$ (Figure 14), which was computed as $\{\boldsymbol{f}_{res}\} = [\mathbf{K}]\{\partial\boldsymbol{v}\}$ (see Equations (5) and (6)). On either scan, similar "bands" as in the gray level residual field are observed. However, the equilibrium gap residual values in the beams and shafts are much lower than the values in the top and bottom parts. The fact that the residuals increased in magnitude from the first to the second scan indicates that nonlinear phenomena, which were penalized, occurred in the latter.

Please cite this document as: M. Valmalle, A. Vintache, B. Smaniotto, F. Gutmann, M. Spagnuolo, A. Ciallella, F. Hild, "Local-global DVC analyses confirm theoretical predictions for deformation and damage onset in torsion of pantographic metamaterial", *Mechanics of Materials* (2022), doi:https://doi.org/10.1016/j.mechmat.2022.104379.

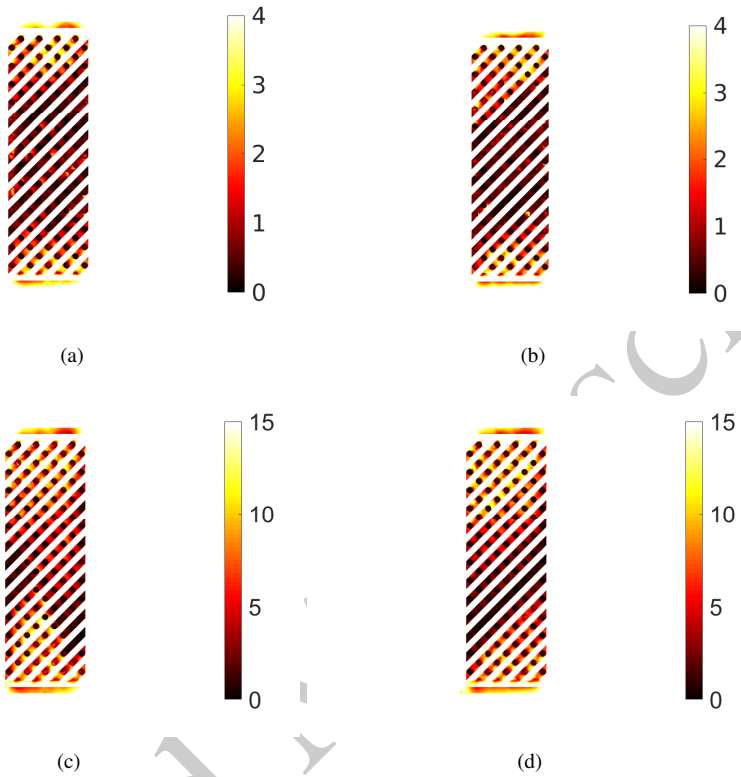

FIGURE 14. Norm of nodal equilibrium residual fields (expressed in arbitrary units) on the front (a,c) and rear (b,d) surfaces for the first (a,b) and second (c,d) deformed scans

In Figure 15(a,c), the displacement fields in the out-of-plane direction are shown for both scans. Their overall amplitude is similar to that observed for the macroscopic mesh (Figure 12(b,e)). However, a lot more details are now available thanks to the fine discretization used herein (Figure 6).

Please cite this document as: M. Valmalle, A. Vintache, B. Smaniotto, F. Gutmann, M. Spagnuolo, A. Ciallella, F. Hild, "Local-global DVC analyses confirm theoretical predictions for deformation and damage onset in torsion of pantographic metamaterial", *Mechanics of Materials* (2022), doi:https://doi.org/10.1016/j.mechmat.2022.104379.

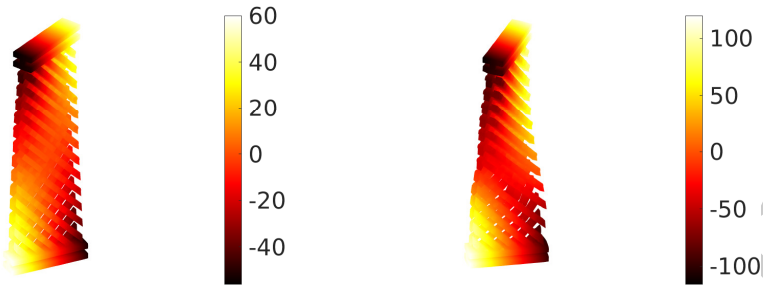

(a) (b)

FIGURE 15. Out-of-plane displacement fields for the first (a) and second (b) deformed scans. The fields are reported on the corresponding deformed configurations and expressed in voxels

The first interesting piece of information is the maximum principal strain field (Figure 16). Multiple strained areas are observed for the first scan (Figure 16(a,b)). However, none of them led to the fracture line, which is visible in Figure 16(c). One family of beams (Figure 16(c)) eventually experienced more deformation than the second one (Figure 16(d)). Conversely, for the first scan, the two families were essentially equally strained with various zones with high levels.

Please cite this document as: M. Valmalle, A. Vintache, B. Smaniotto, F. Gutmann, M. Spagnuolo, A. Ciallella, F. Hild, "Local-global DVC analyses confirm theoretical predictions for deformation and damage onset in torsion of pantographic metamaterial", *Mechanics of Materials* (2022), doi:https://doi.org/10.1016/j.mechmat.2022.104379.

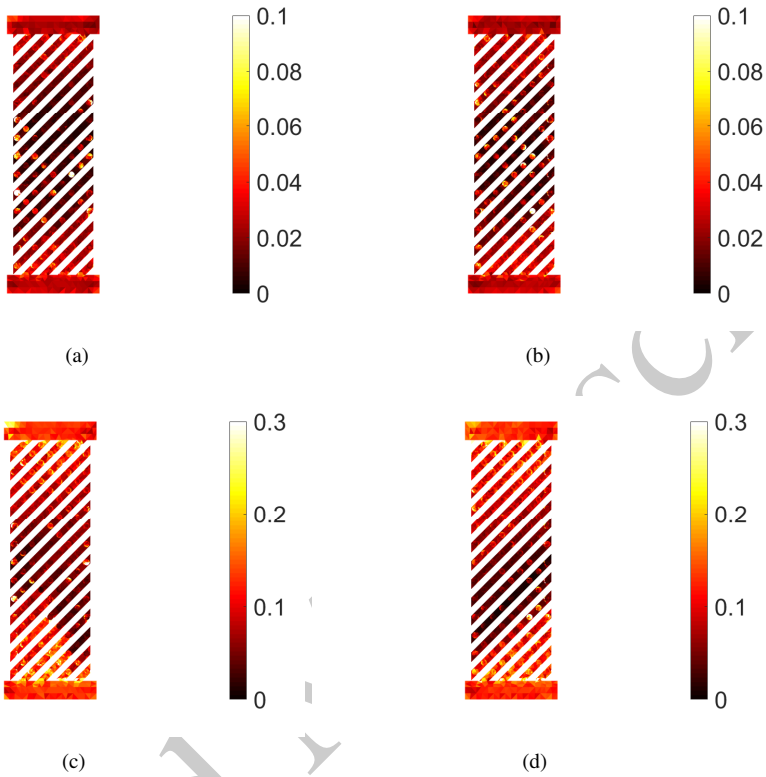

FIGURE 16. Major principal strain fields on the front (a,c) and rear (b,d) surfaces for the first (a,b) and second (c,d) deformed scan

Given that plasticity is the first nonlinear mechanism at play, the equivalent von Mises strain is also reported. It is worth noting that with the reported uncertainties (Table 2), elastic strains could not be measured, thus total and plastic strains could not be distinguished. Comparing Figures 17 and 16, it is concluded that the two strain fields are very similar and that all the features in terms of strained areas are identical. This result is due to the particular mesostructure of the metamaterial and to the fact that very local fields were only partially captured with the present discretization (Figure 6).

Please cite this document as: M. Valmalle, A. Vintache, B. Smaniotto, F. Gutmann, M. Spagnuolo, A. Ciallella, F. Hild, "Local-global DVC analyses confirm theoretical predictions for deformation and damage onset in torsion of pantographic metamaterial", *Mechanics of Materials* (2022), doi:https://doi.org/10.1016/j.mechmat.2022.104379.

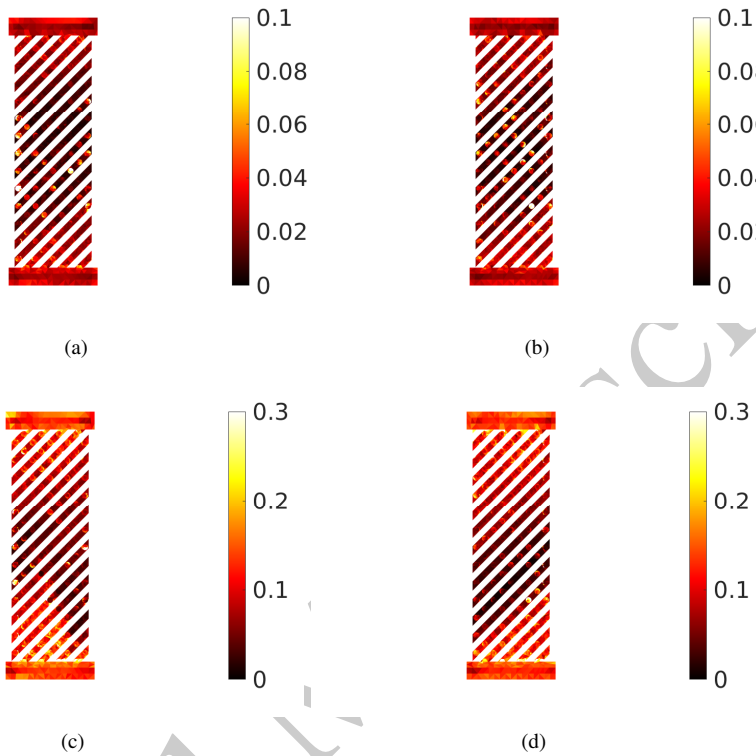

FIGURE 17. Equivalent strain fields on the front (a,c) and rear (b,d) surfaces for the first (a,b) and second (c,d) deformed scans

4.2. **Analysis of the Pivoting Links.** The following discussions focus on the 234 links (Figure 10). Figure 18 shows the norm of the displacement jumps for both faces and deformed configurations. There is no direct correlation between these data and the existence of strained bands (Figures 16 and 17). In particular, for the second deformed scan, the penalization was still enforced even though some displacement jump amplitudes were greater than the nominal clearance on the radius (*i.e.,* 2.4 vx).

Please cite this document as: M. Valmalle, A. Vintache, B. Smaniotto, F. Gutmann, M. Spagnuolo, A. Ciallella, F. Hild, "Local-global DVC analyses confirm theoretical predictions for deformation and damage onset in torsion of pantographic metamaterial", *Mechanics of Materials* (2022), doi:https://doi.org/10.1016/j.mechmat.2022.104379.

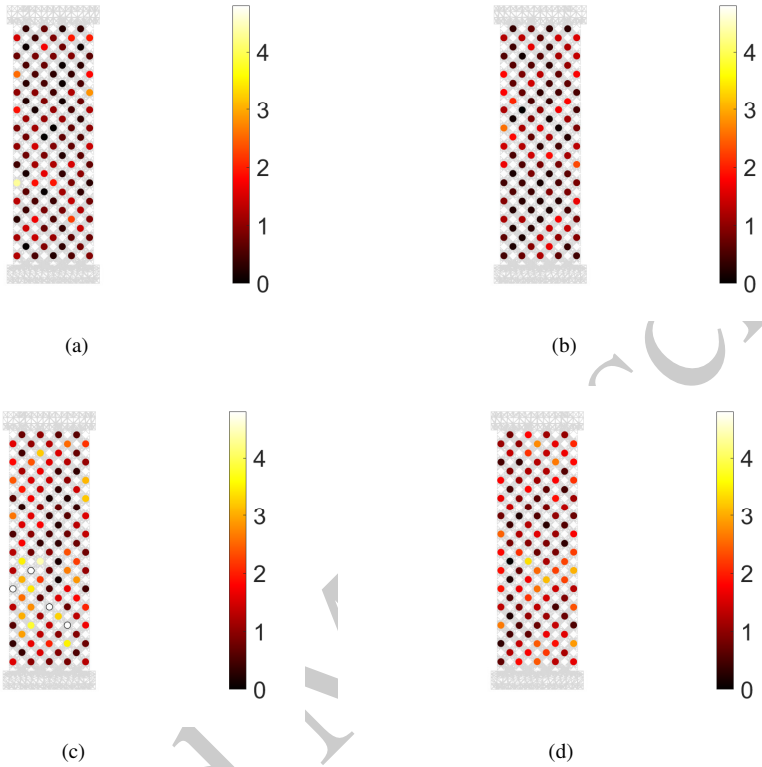

FIGURE 18. Norm of displacement jumps (expressed in voxels) on the front (a,c) and rear (b,d) pivoting links for the first (a,b) and second (c,d) deformed scans. The dynamic range of the plots was limited to two times the observed clearance on the radius (*i.e.,* 4.8 vx)

The distribution of all displacement jump components is displayed in Figure 19. Given the fact that their overall levels were significantly higher than those observed in the uncertainty analysis (Figure 11), the results are possibly trustworthy. For the first scan, very few hinges saw their displacement jump reach the average clearance. Of all components, the highest amplitude was observed in the z-direction for 91 pivots, 79 in the y-direction and 69 in the x-direction. The mean displacement jump norm was equal to 0.8 vx. For the second scan, the norm of displacement jumps increased. Its mean level was equal to 1.5 vx. Some additional links had their displacement jump norm greater than the average clearance. Eighty five pivots had their maximum amplitude along the z-direction, another 85 in the y-direction, and 64 in the x-direction.

Please cite this document as: M. Valmalle, A. Vintache, B. Smaniotto, F. Gutmann, M. Spagnuolo, A. Ciallella, F. Hild, "Local-global DVC analyses confirm theoretical predictions for deformation and damage onset in torsion of pantographic metamaterial", *Mechanics of Materials* (2022), doi:https://doi.org/10.1016/j.mechmat.2022.104379.

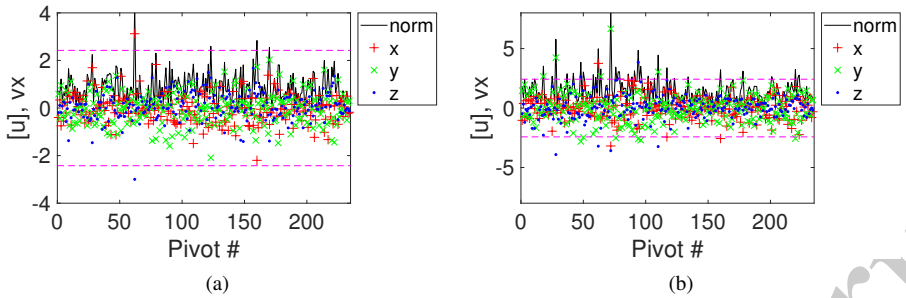

FIGURE 19. Displacement jumps in the 234 pivots for the first (a) and second (b) deformed scans. The horizontal dashed magenta line shows the average clearance on the radius (*i.e.,* 160 μm or 2.4 vx) in the printed configuration (Figure 2(d))

In Figure 20, the norm of displacement jumps of the second deformed scan is plotted as a function of their level in the first deformed scan. Many pivots did not experience very high amplitudes, which is an indication that they were still undamaged. As the applied amplitude was doubled, the displacement jumps increased on average 1.4 times. This observation indicates that some parts of the beams were unloaded because of damage.

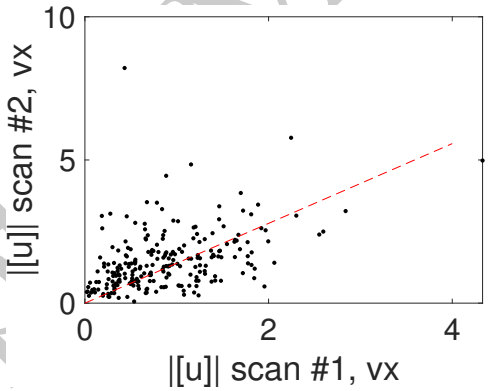

FIGURE 20. Norm of displacement jumps for the second deformed scan as a function of their level in the first deformed scan. The red dashed line shows the linear interpolation

5. DAMAGE ONSET PREDICTION BASED ON A 4-FIELD SECOND GRADIENT CONTINUUM MODEL

In Refs. [45, 31], an enhanced model for pantographic sheets was proposed to predict their behavior when the displacements and rotations of the families of beams could not be described by the same kinematic fields. In other words, the reduced second gradient continuum model to be used in order to get reliable predictions in shorter computational times was a richer kinematics than the model introduced by Steigmann et al. [1]. In that paper, the authors assumed that the interconnecting hinges were "strong enough" to prescribe equal displacements and rotations to the beam sections they connect. In torsion, the model to be used should be able to describe the expected deformation of hinges in Poynting effects

Please cite this document as: M. Valmalle, A. Vintache, B. Smaniotto, F. Gutmann, M. Spagnuolo, A. Ciallella, F. Hild, "Local-global DVC analyses confirm theoretical predictions for deformation and damage onset in torsion of pantographic metamaterial", *Mechanics of Materials* (2022), doi:https://doi.org/10.1016/j.mechmat.2022.104379.

when large amplitude twist occurs. It is worth mentioning that peridynamics may also be efficient as a theoretical guide [46, 47].

In the present section, the model proposed by Giorgio et al. [45, 31] will be utilized to investigate the experimental evidence reported above. It is believed to be exhaustive enough to predict the deformation phenomena experienced by perfect hinges, and simple enough to require short time computations. The present study refrained from modeling pantographic sheets as 3D Cauchy continua with a reference configuration having a complex geometry (and contact would need to be accounted for) or as a lattice of constrained beams. Such refined models are computationally expensive [48, 49, 50]. The modeling choice made herein revealed to be very convenient as numerical simulations took only 10 minutes by using a suitably designed commercial code.

The reduced order model [45, 31] has a kinematics that is believed to be rich enough to describe the loadings prescribed to the hinges by the connected beams. Moreover, it easily describes perfect hinges by equating to zero the stiffness k_γ in Equation (13) relative to shear of the two arrays of beams (see Equation (11)). The following deformation measures for the fibers and the hinges are introduced to express the strain energy of the pantographic metamaterial [31]

$$
\begin{aligned}
{}^{\alpha}\boldsymbol{e} &= \left({}^{\alpha}\varepsilon, {}^{\alpha}\gamma_p, {}^{\alpha}\gamma_n\right), \quad {}^{\alpha}\boldsymbol{\kappa} = \left({}^{\alpha}\kappa_t, {}^{\alpha}\kappa_n, {}^{\alpha}\kappa_g\right) && (9)\\
{}^{c}\boldsymbol{e} &= \left({}^{c}\gamma_1, {}^{c}\gamma_2, {}^{c}\varepsilon\right), \quad {}^{c}\boldsymbol{\kappa} = \left({}^{c}\kappa_1, {}^{c}\kappa_2, {}^{c}\kappa_t\right) && (10)
\end{aligned}
$$

and represent the elongations ${}^{\alpha}\varepsilon$, the shears along the in-plane ${}^{\alpha}\gamma_p$, and the out-of-plane direction ${}^{\alpha}\gamma_n$, the torsions ${}^{\alpha}\kappa_t$, and the normal ${}^{\alpha}\kappa_n$, and geodesic ${}^{\alpha}\kappa_g$ curvatures for the fibers; the shears along the in-plane directions ${}^{c}\gamma_1$ and ${}^{c}\gamma_2$, the elongation ${}^{c}\varepsilon$, the curvatures along the in-plane directions ${}^{c}\kappa_1$ and ${}^{c}\kappa_2$, and the torsion ${}^{c}\kappa_t$ for the connections due to the hinges. Given these measures of deformation, it was assumed that the strain energy density was a quadratic form with two separate contributions relative to the fibers and the hinges [31]

$$
\pi\left({}^{\alpha}\boldsymbol{e}, {}^{c}\boldsymbol{e}, {}^{\alpha}\boldsymbol{\kappa}, {}^{c}\boldsymbol{\kappa}\right) = \pi_f\left({}^{\alpha}\boldsymbol{e}, {}^{\alpha}\boldsymbol{\kappa}\right) + \pi_c\left({}^{c}\boldsymbol{e}, {}^{c}\boldsymbol{\kappa}\right) \tag{11}
$$

with

$$
\begin{aligned}
\pi_f\left({}^{\alpha}\boldsymbol{e}, {}^{\alpha}\boldsymbol{\kappa}\right) &= \frac{1}{2}\Big[{}^{f}k_e({}^{1}\varepsilon^2 + {}^{2}\varepsilon^2) + k_{\gamma_p}({}^{1}\gamma_p^2 + {}^{2}\gamma_p^2) + k_{\gamma_n}({}^{1}\gamma_n^2 + {}^{2}\gamma_n^2)\\
&+ {}^{f}k_\tau({}^{1}\kappa_\tau^2 + {}^{2}\kappa_\tau^2) + k_n({}^{1}\kappa_n^2 + {}^{2}\kappa_n^2) + k_g({}^{1}\kappa_g^2 + {}^{2}\kappa_g^2)\Big] && (12)\\
\pi_c\left({}^{c}\boldsymbol{e}, {}^{c}\boldsymbol{\kappa}\right) &= \frac{1}{2}\left[{}^{c}k_e\,{}^{c}\varepsilon^2 + k_\gamma({}^{c}\gamma_1^2 + {}^{c}\gamma_2^2) + k_{\gamma_b}({}^{c}\gamma_1^2 + {}^{c}\gamma_2^2) + {}^{c}k_\tau\,{}^{c}\kappa_\tau^2\right] && (13)
\end{aligned}
$$

where the material parameters ${}^{f}k_e$, k_{γ_p}, k_{γ_n}, ${}^{f}k_\tau$, k_n and k_g are positive constants, assumed to be equal for the two fiber families, and represent the stiffnesses related to the elongation, in-plane and out-of-plane shear, twist, normal and geodesic bending, respectively. Moreover, ${}^{c}k_e$, k_γ, k_{γ_b} and ${}^{c}k_\tau$ are positive constants related to the elongation, torsion, shear and bending stiffnesses of the hinges. The constitutive parameters were estimated with the 3D geometry of the pantographic sheet in the reference configuration [31]. The key parameters were hinge dimensions, beam section shape and dimensions, distance between beams, elastic moduli of the printed material. First estimates were obtained via homogenization, and subsequent corrections [31], which were due to the fact that 3D printed materials have granular mesostructures (Figure 2(c)). The ten calibrated parameters are gathered in Table 3.

Please cite this document as: M. Valmalle, A. Vintache, B. Smaniotto, F. Gutmann, M. Spagnuolo, A. Ciallella, F. Hild, "Local-global DVC analyses confirm theoretical predictions for deformation and damage onset in torsion of pantographic metamaterial", *Mechanics of Materials* (2022), doi:https://doi.org/10.1016/j.mechmat.2022.104379.

TABLE 3. Calibrated stiffnesses of the selected model [45, 31]

Fibers	value	Hinges	value
${}^{f}k_e$	3.3 N/m	${}^{c}k_e$	4.5 N/m^3
k_{γ_p}	1.6×10^6 N/m	k_γ	2.8 N/m^3
k_{γ_n}	1.6×10^6 N/m	k_{γ_b}	1.1 N/m
${}^{f}k_\tau$	36.2 J	${}^{c}k_\tau$	0 N/m
k_n	11.8 J		
k_g	2.4 J		

The numerical simulation was carried out up to the angle of rotation at which the first load drop of the pantographic structure occurred (Figure 4) as the model included neither damage nor plasticity. A step toward the modeling of these mechanisms can be found in Refs. [51, 52]. Since one of the interests of the torsion test lied in the fact that it exhibited a Poynting effect (Figure 4(b)), it was important to be able to have a numerical estimate of the reaction force and a prediction of the deformed shapes in an prescribed angular twist test. In Figure 21(a), the torque predicted by numerical simulation is compared to the experimental measurements, and in Figure 21(b) the corresponding reaction forces. There is a qualitative agreement, and in the purely elastic part a good quantitative coincidence. It is worth noting that both reaction force and torque have been computed by means of Castigliano's theorem [53]. If one has access to the global strain energy of the metamaterial for each deformation step, then the force is computed as the finite difference between the energies associated with two successive deformation steps divided by the corresponding prescribed displacement. This procedure produces $n-1$ force (or torque) values for n strain energies given. This is the reason offset corresponding to angle 0 is observed in both plots. Furthermore, the estimates found for the reaction force and torque result from an effort to obtain acceptable estimates of both curves and the deformed shapes of the metamaterial.

It is observed that an inverse Poynting effect was activated in the initial part of the test (Figures 4 and 21). The Poynting effect is related to the interplay between fiber extensional and hinge deformation energies. The most crucial parameters are therefore ${}^{f}k_e$, ${}^{c}k_e$, k_γ and k_{γ_b}.

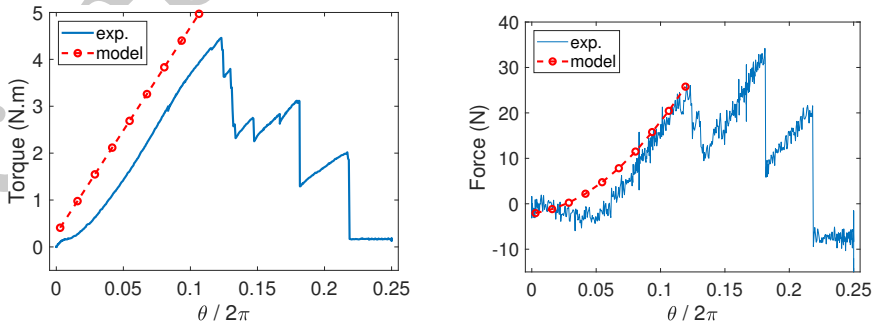

FIGURE 21. Experimental and predicted torques (a), induced normal forces (b)

Figure 22 displays the deformed shapes of the middle surfaces obtained via numerical simulations and from the experiment. The experimental surfaces pass through the centers

Please cite this document as: M. Valmalle, A. Vintache, B. Smaniotto, F. Gutmann, M. Spagnuolo, A. Ciallella, F. Hild, "Local-global DVC analyses confirm theoretical predictions for deformation and damage onset in torsion of pantographic metamaterial", *Mechanics of Materials* (2022), doi:https://doi.org/10.1016/j.mechmat.2022.104379.

of mass of the pivoting links. Both pairs of surfaces are plotted for an angular amplitude of $\theta = 0.75$ rad. A qualitative agreement is also achieved for the deformed shapes of the metamaterial. It is important to have a model that is capable to predict both the load response and the deformed shape of the metamaterial. Depending on the type of applications in which the pantographic metamaterial is to be used, it will not only be necessary to be able to provide quantitative predictions of the mechanical response in torsion (or other tests), but also to have estimates of the deformed shape.

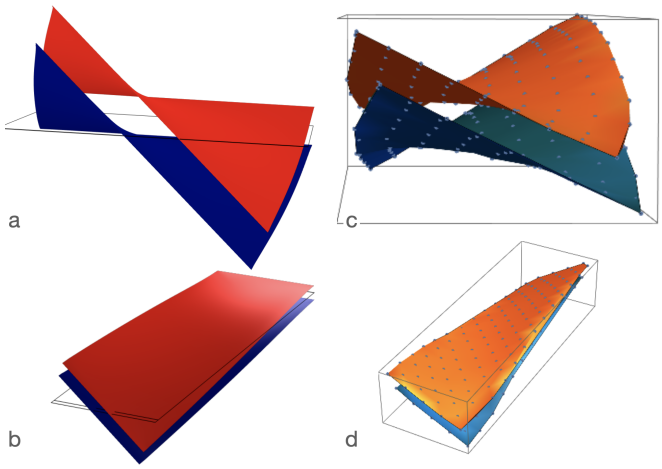

FIGURE 22. Comparison between the deformed shapes of the middle surfaces obtained via numerical simulations (a,b) and from the experiment (c,d). The experimental surfaces (c,d) are plotted on the measured positions of the centers of mass of each pivoting link

A useful criterion for predicting damage sites is the observation of the portions of the metamaterial in which there is a higher density of strain energy. Figures 23-25 show plots of, respectively, deformation measures for the geodesic curvature (*i.e.,* the curvature of the fibers on the surface identified by the fibers themselves), normal curvature (*i.e.,* the curvature of the fibers normal to the surface identified by the fibers themselves) and twist (*i.e.,* the torsion of the fibers along their axis). All these deformation measures were introduced in Equation (9) and are discussed in detail in Ref. [31]. In Fig. 23, the predicted deformed configuration of the two fiber layers is shown. The colors represent the predicted geodesic curvature. Three zones are identified. In the central zone, the geodesic curvature is negligibly small. Conversely, in the two lateral regions, symmetrically positive and negative curvatures are observed. This distribution can be interpreted as an interface phenomenon, which is induced by the proximity of the boundaries.

Please cite this document as: M. Valmalle, A. Vintache, B. Smaniotto, F. Gutmann, M. Spagnuolo, A. Ciallella, F. Hild, "Local-global DVC analyses confirm theoretical predictions for deformation and damage onset in torsion of pantographic metamaterial", *Mechanics of Materials* (2022), doi:https://doi.org/10.1016/j.mechmat.2022.104379.

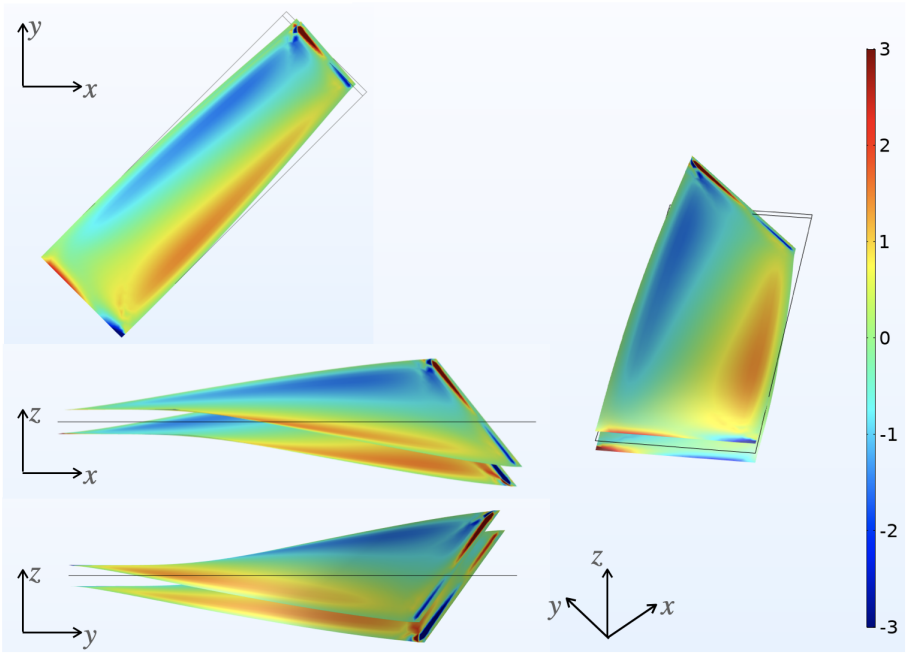

FIGURE 23. Four different views for the geodesic curvature plotted on the deformed shapes of the two middle surfaces when $\theta = 0.75$ rad. The measure of deformation is plotted in color scale and expressed in $1/m$

In Fig. 24, the predicted normal curvature is displayed on the deformed configuration. A large central zone is surrounded by boundary layers. In the latter ones, the maximum level of normal curvature is reached. Due to clamping boundary conditions on the short sides of the metamaterial, higher normal curvatures occurred on parts of them, while negligible normal curvature were present in the other part of the short sides and on long sides.

Please cite this document as: M. Valmalle, A. Vintache, B. Smaniotto, F. Gutmann, M. Spagnuolo, A. Ciallella, F. Hild, "Local-global DVC analyses confirm theoretical predictions for deformation and damage onset in torsion of pantographic metamaterial", *Mechanics of Materials* (2022), doi:https://doi.org/10.1016/j.mechmat.2022.104379.

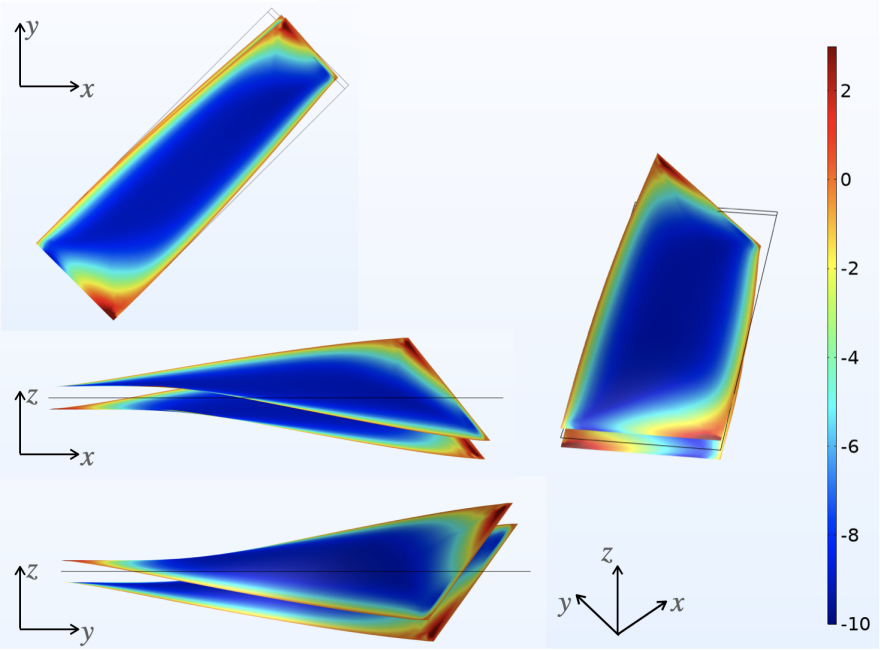

FIGURE 24. Four different views for the normal curvature plotted on the deformed shapes of the two middle surfaces when $\theta = 0.75$ rad. The measure of deformation is plotted in color scale and expressed in $1/m$

Figure 25 shows the predicted fiber twist. A band deformation pattern is observed. In the central zone virtually no twist is predicted. Conversely, in opposite corners, a high concentration of twist is forecast. Two bands of concentrated twist are also observed along the long sides and a transverse band connects the highly deformed corner with the opposite long side along the fiber direction.

Please cite this document as: M. Valmalle, A. Vintache, B. Smaniotto, F. Gutmann, M. Spagnuolo, A. Ciallella, F. Hild, "Local-global DVC analyses confirm theoretical predictions for deformation and damage onset in torsion of pantographic metamaterial", *Mechanics of Materials* (2022), doi:https://doi.org/10.1016/j.mechmat.2022.104379.

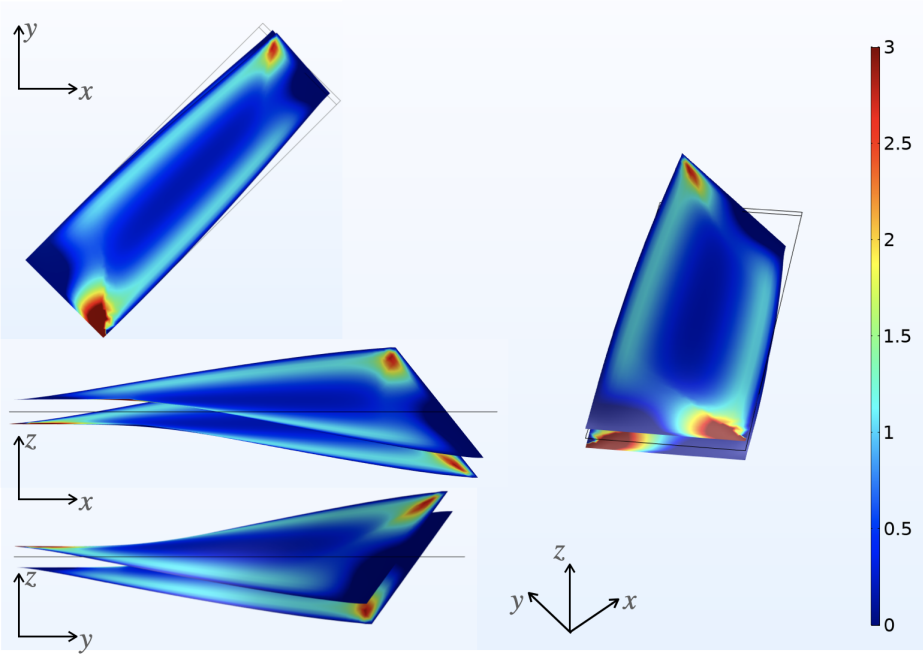

FIGURE 25. Four different views for the twist plotted on the deformed shapes of the two middle surfaces when $\theta = 0.75$ rad. The measure of deformation is plotted in color scale and expressed in $1/m$

Two placement fields describe the kinematics of the pantographic sheet, one for each beam family. Therefore, the deformation of each hinge is predicted by comparing relative displacements and rotations of the corresponding material points. Figure 26 displays the gradient of the difference of geodesic curvatures for the two families of fibers for selected angular amplitudes. Due to the specific geometry of the metamaterial tested herein (*i.e.,* presence of bores to obtain perfect hinges), it was expected that damage would not occur in the hinges but in the corresponding hinge bores (in the beams). These bores were necessary in order to link the hinge shafts with the beams (Figure 2), and their presence made the interconnected beams less resistant. It was envisioned that damage may occur at locations where geodesic bending of the fibers was maximum since this deformation mode produces high strains in the vicinity of bores. Figure 26 shows the pattern of geodesic curvature difference to be expected in the elastic regime of a torsion test. The blue/red colored crosses starting from the short sides and moving toward the central part of the specimen while the twist angle increases determine the expected damage localization sites, which is suggestive of the experimental evidence shown in Figure 3.

Please cite this document as: M. Valmalle, A. Vintache, B. Smaniotto, F. Gutmann, M. Spagnuolo, A. Ciallella, F. Hild, "Local-global DVC analyses confirm theoretical predictions for deformation and damage onset in torsion of pantographic metamaterial", *Mechanics of Materials* (2022), doi:https://doi.org/10.1016/j.mechmat.2022.104379.

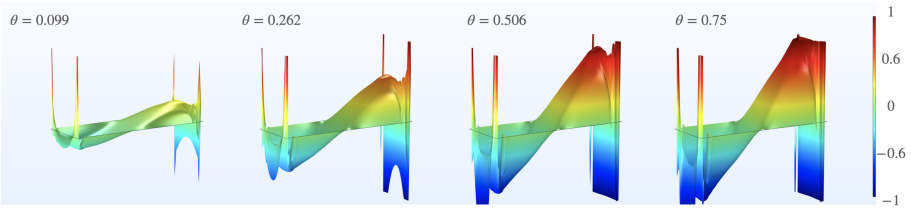

FIGURE 26. Plot of the difference of geodesic curvature (expressed in $1/m$) for different torsion angles (expressed in rad)

This numerical analysis proves that a failure criterion linking bore fracture to geodesic curvature difference and its gradient is consistent with experimental observations. For more in-depth examination, a damage threshold written in terms of differences between geodesic curvatures is to be further probed. This analysis can be conducted using the same pattern introduced in Ref. [52] to describe the onset of damage for pantographic structures with plastic hinges.

6. CONCLUSION

An in situ torsion test was performed on a pantographic metamaterial in which perfect hinges were fabricated via additive manufacturing. A local-global DVC framework was implemented to explicitly measure the deformation of the 3D printed links. Multiple point constraints were implemented with an additional penalty term in the DVC cost function to account for the presence of clearances between the shafts and the beams. Consequently, each independent meshed part was weakly linked to its complementary counterpart to recreate pivoting joints. Such algorithm was validated with the in situ torsion test discussed herein.

Since finite-element DVC was considered, a mesh was constructed from the CAD model of the printed metamaterial. This mesh had to be fitted onto the printed configuration. A DVC-based backtracking procedure was followed in which the voxelized twin was constructed using its STL description and a ray tracing implementation. Further, DVC had to be initialized since large angular amplitudes were considered between two acquisitions. No contrast was observed in the printed metamaterial (*i.e.,* no major internal defects appeared for the selected resolution). Regularized DVC was therefore utilized with an equilibrium gap functional based upon Hencky elasticity.

With all these new features, DVC analyses were deemed successful. In particular, the penalization of displacement jumps at each pivoting link was shown to be effective in capturing the overall kinematics of the *in situ* torsion test. Even though the displacement jumps were penalized, they gave interesting indicates on damage development. The strain fields and gray level residuals enabled some of the damaged zones to be detected. Last, the growth of damage was sudden and the final fracture zone could not be located in the intermediate scan, which showed strained zones that turned out not to coincide with the fully damaged area. This last observation shows that the temporal sampling was too poor to monitor damage inception and growth.

In order to design further experiments, which is necessary to fully understand and quantify the damage mechanisms of pantographic metamaterials in torsional deformation, the model developed by Giorgio et al. [31] was adopted. This model was rich enough to account for the deformations prescribed to the interconnecting hinges prior to damage initiation. The modeling hypotheses were based on the peculiar strain energy features in

Please cite this document as: M. Valmalle, A. Vintache, B. Smaniotto, F. Gutmann, M. Spagnuolo, A. Ciallella, F. Hild, "Local-global DVC analyses confirm theoretical predictions for deformation and damage onset in torsion of pantographic metamaterial", *Mechanics of Materials* (2022), doi:https://doi.org/10.1016/j.mechmat.2022.104379.

the considered test. The introduction of a damage criterion based on the geodesic curvature difference of the two fiber families was suggested. Based on the data gathered from the present test, and on a suitably implemented numerical model, it will be possible to design the next campaign of torsional tests also taking into account the possibility of investigating optimized metamaterials [54, 55, 56] in order to exploit the Poynting effect for given applications, as the influence of friction and plasticity in static and dynamic phenomena involving pantographic structures [57, 58, 59, 60, 61].

Acknowledgments

This work has been partially supported by the French "Agence Nationale de la Recherche" through the "Investissements d'avenir" program (ANR-10-EQPX-37 MATMECA Grant). MS was supported by P.O.R. Sardegna F.S.E. 2014-2020 Asse III: Istruzione e Formazione, Obiettivo Tematico: 10, Obiettivo Specifico: 10.5, Azione dell,Äôaccordo di Partenariato:10.5.12 - Avviso di chiamata per il finanziamento di Progetti di ricerca, Anno 2017 (CUP F24J17000190009).

References

[1] D. J. Steigmann and F. dell'Isola, "Mechanical response of fabric sheets to three-dimensional bending, twisting, and stretching," *Acta Mechanica Sinica*, vol. 31, no. 3, pp. 373–382, 2015.

[2] I. Giorgio, R. Grygoruk, F. dell'Isola, and D. J. Steigmann, "Pattern formation in the three-dimensional deformations of fibered sheets," *Mechanics Research Communications*, vol. 69, pp. 164–171, 2015.

[3] F. dell'Isola and D. Steigmann, "A two-dimensional gradient-elasticity theory for woven fabrics," *Journal of Elasticity*, vol. 118, no. 1, pp. 113–125, 2015.

[4] A. Carcaterra, F. dell'Isola, R. Esposito, and M. Pulvirenti, "Macroscopic description of microscopically strongly inhomogenous systems: A mathematical basis for the synthesis of higher gradients metamaterials," *Archive for Rational Mechanics and Analysis*, vol. 218, no. 3, pp. 1239–1262, 2015.

[5] F. dell'Isola, D. Steigmann, and A. Della Corte, "Synthesis of fibrous complex structures: designing microstructure to deliver targeted macroscale response," *Applied Mechanics Reviews*, vol. 67, no. 6, pp. 21–pages, 2016.

[6] F. dell'Isola, I. Giorgio, M. Pawlikowski, and N. L. Rizzi, "Large deformations of planar extensible beams and pantographic lattices: heuristic homogenization, experimental and numerical examples of equilibrium," *Proceedings of the Royal Society A: Mathematical, Physical and Engineering Sciences*, vol. 472, no. 2185, p. 20150790, 2016.

[7] E. Turco, "A numerical survey of nonlinear dynamical responses of discrete pantographic beams," *Continuum Mechanics and Thermodynamics*, pp. 1–21, 2021.

[8] E. Turco, A. Misra, M. Pawlikowski, F. dell'Isola, and F. Hild, "Enhanced piola–hencky discrete models for pantographic sheets with pivots without deformation energy: numerics and experiments," *International Journal of Solids and Structures*, vol. 147, pp. 94–109, 2018.

[9] U. Andreaus, F. dell'Isola, I. Giorgio, L. Placidi, T. Lekszycki, and N. L. Rizzi, "Numerical simulations of classical problems in two-dimensional (non) linear second gradient elasticity," *International Journal of Engineering Science*, vol. 108, pp. 34–50, 2016.

[10] F. dell'Isola, P. Seppecher, and A. Madeo, "How contact interactions may depend on the shape of cauchy cuts in n-th gradient continua: approach" à la d'alembert"," *Zeitschrift für angewandte Mathematik und Physik*, vol. 63, no. 6, pp. 1119–1141, 2012.

[11] F. dell'Isola and P. Seppecher, "Edge contact forces and quasi-balanced power," *Meccanica*, vol. 32, no. 1, pp. 33–52, 1997.

[12] P. Seppecher, J.-J. Alibert, and F. dell'Isola, "Linear elastic trusses leading to continua with exotic mechanical interactions," in *Journal of Physics: Conference Series*, vol. 319, p. 012018, IOP Publishing, 2011.

[13] J.-J. Alibert, P. Seppecher, and F. dell'Isola, "Truss modular beams with deformation energy depending on higher displacement gradients," *Mathematics and Mechanics of Solids*, vol. 8, no. 1, pp. 51–73, 2003.

[14] V. A. Eremeyev, F. dell'Isola, C. Boutin, and D. Steigmann, "Linear pantographic sheets: existence and uniqueness of weak solutions," *Journal of Elasticity*, vol. 132, no. 2, pp. 175–196, 2018.

[15] P. Germain, "The method of virtual power in the mechanics of continuous media, I: Second-gradient theory," *Mathematics and Mechanics of Complex Systems*, vol. 8, no. 2, pp. 153–190, 2020.

Please cite this document as: M. Valmalle, A. Vintache, B. Smaniotto, F. Gutmann, M. Spagnuolo, A. Ciallella, F. Hild, "Local-global DVC analyses confirm theoretical predictions for deformation and damage onset in torsion of pantographic metamaterial", *Mechanics of Materials* (2022), doi:https://doi.org/10.1016/j.mechmat.2022.104379.

[16] N. Auffray, F. dell'Isola, V. A. Eremeyev, A. Madeo, and G. Rosi, "Analytical continuum mechanics à la hamilton–piola least action principle for second gradient continua and capillary fluids," *Mathematics and Mechanics of Solids*, vol. 20, no. 4, pp. 375–417, 2015.

[17] V. A. Eremeyev, F. S. Alzahrani, A. Cazzani, F. dell'Isola, T. Hayat, E. Turco, and V. Konopińska-Zmysłowska, "On existence and uniqueness of weak solutions for linear pantographic beam lattices models," *Continuum Mechanics and Thermodynamics*, vol. 31, no. 6, pp. 1843–1861, 2019.

[18] M. Cuomo, F. dell'Isola, and L. Greco, "Simplified analysis of a generalized bias test for fabrics with two families of inextensible fibres," *Zeitschrift für angewandte Mathematik und Physik*, vol. 67, no. 3, p. 61, 2016.

[19] M. Cuomo, F. dell'Isola, L. Greco, and N. Rizzi, "First versus second gradient energies for planar sheets with two families of inextensible fibres: investigation on deformation boundary layers, discontinuities and geometrical instabilities," *Composites Part B: Engineering*, vol. 115, pp. 423–448, 2017.

[20] F. dell'Isola, M. Cuomo, L. Greco, and A. Della Corte, "Bias extension test for pantographic sheets: numerical simulations based on second gradient shear energies," *Journal of Engineering Mathematics*, pp. 1–31, 2016.

[21] F. dell'Isola, M. V. d'Agostino, A. Madeo, P. Boisse, and D. Steigmann, "Minimization of shear energy in two dimensional continua with two orthogonal families of inextensible fibers: The case of standard bias extension test," *Journal of Elasticity*, pp. 25–pages, 2015.

[22] F. dell'Isola, T. Lekszycki, M. Pawlikowski, R. Grygoruk, and L. Greco, "Designing a light fabric metamaterial being highly macroscopically tough under directional extension: first experimental evidence," *Zeitschrift für angewandte Mathematik und Physik*, vol. 66, no. 6, pp. 3473–3498, 2015.

[23] J. Poynting, "XXXIX. Radiation pressure," *The London, Edinburgh, and Dublin Philosophical Magazine and Journal of Science*, vol. 9, no. 52, pp. 393–406, 1905.

[24] A. Misra, T. Lekszycki, I. Giorgio, G. Ganzosch, W. Müller, and F. dell'Isola, "Pantographic metamaterials show atypical Poynting effect reversal," *Mechanics Research Communications*, vol. 89, pp. 6–10, 2018.

[25] P. Auger, T. Lavigne, B. Smaniotto, M. Spagnuolo, F. dell'Isola, and F. Hild, "Poynting Effects in Pantographic Metamaterial Captured via Multiscale DVC," *Journal of Strain Analysis for Engineering Design*, 2021.

[26] J. Poynting, "On pressure perpendicular to the shear planes in finite pure shears , and on the lengthening of loaded wires when twisted," *Proceedings of the Royal Society of London*, vol. A82, no. 557, pp. 546–559, 1909.

[27] J. Poynting, "The changes in length and volume of an Indian-rubber cord when twisted," *India-Rubber Journal*, vol. October 4, p. 6, 1913.

[28] B. Bay, T. Smith, D. Fyhrie, and M. Saad, "Digital volume correlation: three-dimensional strain mapping using X-ray tomography," *Experimental Mechanics*, vol. 39, pp. 217–226, 1999.

[29] B. Bay, "Methods and applications of digital volume correlation," *Journal of Strain Analysis for Engineering Design*, vol. 43, pp. 745–760, 2008.

[30] S. Roux, F. Hild, P. Viot, and D. Bernard, "Three dimensional image correlation from X-Ray computed tomography of solid foam," *Composites Part A: Applied Science and Manufacturing*, vol. 39, no. 8, pp. 1253–1265, 2008.

[31] I. Giorgio, V. Varano, F. dell'Isola, and N. L. Rizzi, "Two layers pantographs: a 2d continuum model accounting for the beams,Äô offset and relative rotations as averages in so (3) lie groups," *International Journal of Solids and Structures*, vol. 216, pp. 43–58, 2021.

[32] E. Maire and P. J. Withers, "Quantitative X-ray tomography," *International Materials Reviews*, vol. 59, no. 1, pp. 1–43, 2014.

[33] J. Buffière, E. Maire, J. Adrien, J. Masse, and E. Boller, "In Situ Experiments with X ray Tomography: an Attractive Tool for Experimental Mechanics," *Experimental Mechanics*, vol. 50, no. 3, pp. 289–305, 2010.

[34] F. Hild, A. Bouterf, L. Chamoin, F. Mathieu, J. Neggers, F. Pled, Z. Tomičević, and S. Roux, "Toward 4D Mechanical Correlation," *Advanced Modeling and Simulation in Engineering Sciences*, vol. 3, no. 1, pp. 1–26, 2016.

[35] T. Taillandier-Thomas, S. Roux, T. Morgeneyer, and F. Hild, "Localized strain field measurement on laminography data with mechanical regularization," *Nuclear Instruments and Methods in Physics Research Section B*, vol. 324, pp. 70–79, 2014.

[36] F. dell'Isola, P. Seppecher, M. Spagnuolo, E. Barchiesi, F. Hild, T. Lekszycki, I. Giorgio, L. Placidi, U. Andreaus, M. Cuomo, S. Eugster, A. Pfaff, K. Hoschke, R. Langkemper, E. Turco, R. Sarikaya, A. Misra, M. De Angelo, F. D'Annibale, A. Bouterf, X. Pinelli, A. Misra, B. Desmorat, M. Pawlikowski, C. Dupuy, D. Scerrato, P. Peyre, M. Laudato, L. Manzari, P. Göransson, C. Hesch, S. Hesch, P. Franciosi, J. Dirrenberger, F. Maurin, Z. Vangelatos, C. Grigoropoulos, V. Melissinaki, M. Farsari, W. Muller, E. Abali, C. Liebold, G. Ganzosch, P. Harrison, R. Drobnicki, L. Igumnov, F. Alzahrani, and T. Hayat, "Advances in Pantographic Structures: Design, Manufacturing, Models, Experiments and Image Analyses," *Continuum Mechanics and Thermodynamics*, vol. 31, no. 4, pp. 1231–1282, 2019.

Please cite this document as: M. Valmalle, A. Vintache, B. Smaniotto, F. Gutmann, M. Spagnuolo, A. Ciallella, F. Hild, "Local-global DVC analyses confirm theoretical predictions for deformation and damage onset in torsion of pantographic metamaterial", *Mechanics of Materials* (2022), doi:https://doi.org/10.1016/j.mechmat.2022.104379.

[37] D. Claire, F. Hild, and S. Roux, "A finite element formulation to identify damage fields: The equilibrium gap method," *Int. J. Num. Meth. Engng.*, vol. 61, no. 2, pp. 189–208, 2004.
[38] S. Patil and B. Ravi, "Voxel-based representation, display and thickness analysis of intricate shapes," in *Ninth International Conference on Computer Aided Design and Computer Graphics (CAD-CG'05)*, pp. 6 pp.–, 2005.
[39] A. Kak and M. Slaney, *Principles of Computerized Tomographic Imaging*. 2001.
[40] C. Caldeira de Melo, M. Furlan, F. Hild, N. Schmitt, and R. Canto, "Uniaxial compression test on ceramic green compact with bending consideration using digital image correlation," *Powder Technology*, vol. 376, pp. 136–148, 2020.
[41] F. Hild, A. Misra, and F. dell'Isola, "Multiscale DIC applied to Pantographic Structures," *Experimental Mechanics*, vol. 61, pp. 431–443, 2021.
[42] L. Jendele and J. Červenka, "On the solution of multi-point constraints–application to FE analysis of reinforced concrete structures," *Computers & Structures*, vol. 87, no. 15-16, pp. 970–980, 2009.
[43] R. D. Cook, D. S. Malkus, M. E. Plesha, and R. J. Witt, *Concepts and Applications of Finite Element Analysis*. Wiley, 4 ed., 2001.
[44] H. Leclerc, J. Neggers, F. Mathieu, F. Hild, and S. Roux, *Correli 3.0*. IDDN.FR.001.520008.000.S.P.2015.000.31500, Agence pour la Protection des Programmes, Paris (France), 2015.
[45] I. Giorgio, N. L. Rizzi, U. Andreaus, and D. J. Steigmann, "A two-dimensional continuum model of pantographic sheets moving in a 3d space and accounting for the offset and relative rotations of the fibers," *Mathematics and Mechanics of Complex Systems*, vol. 7, no. 4, pp. 311–325, 2019.
[46] M. Imachi, S. Tanaka, M. Ozdemir, T. Q. Bui, S. Oterkus, and E. Oterkus, "Dynamic crack arrest analysis by ordinary state-based peridynamics," *International Journal of Fracture*, vol. 221, no. 2, pp. 155–169, 2020.
[47] B. Vazic, H. Wang, C. Diyaroglu, S. Oterkus, and E. Oterkus, "Dynamic propagation of a macrocrack interacting with parallel small cracks," *AIMS Materials Science*, vol. 4, no. 1, pp. 118–136, 2017.
[48] I. Giorgio, "Numerical identification procedure between a micro-cauchy model and a macro-second gradient model for planar pantographic structures," *Zeitschrift für angewandte Mathematik und Physik*, vol. 67, no. 4, pp. 1–17, 2016.
[49] A. Cazzani, M. Malagù, and E. Turco, "Isogeometric analysis of plane-curved beams," *Mathematics and Mechanics of Solids*, vol. 21, no. 5, pp. 562–577, 2016.
[50] C. Hesch, S. Schuß, M. Dittmann, S. Eugster, M. Favino, and R. Krause, "Variational space–time elements for large-scale systems," *Computer Methods in Applied Mechanics and Engineering*, vol. 326, pp. 541–572, 2017.
[51] M. Spagnuolo, K. Barcz, A. Pfaff, F. dell'Isola, and P. Franciosi, "Qualitative pivot damage analysis in aluminum printed pantographic sheets: numerics and experiments," *Mechanics Research Communications*, vol. 83, pp. 47–52, 2017.
[52] M. Spagnuolo, M. E. Yildizdag, X. Pinelli, A. Cazzani, and F. Hild, "Out-of-plane deformation reduction via inelastic hinges in fibrous metamaterials and simplified damage approach," *Mathematics and Mechanics of Solids*, 2022.
[53] J. H. Argyris, "Energy theorems and structural analysis: A generalized discourse with applications on energy principles of structural analysis including the effects of temperature and non-linear stress-strain relations," *Aircraft Engineering and Aerospace Technology*, 1954.
[54] A. Cazzani and M. Rovati, "Sensitivity analysis and optimum design of elastic-plastic structural systems," *Meccanica*, vol. 26, no. 2, pp. 173–178, 1991.
[55] B. Desmorat, M. Spagnuolo, and E. Turco, "Stiffness optimization in nonlinear pantographic structures," *Mathematics and Mechanics of Solids*, vol. 25, no. 12, pp. 2252–2262, 2020.
[56] I. Giorgio, "Lattice shells composed of two families of curved kirchhoff rods: an archetypal example, topology optimization of a cycloidal metamaterial," *Continuum Mechanics and Thermodynamics*, vol. 33, no. 4, pp. 1063–1082, 2021.
[57] A. Ciallella, D. Pasquali, M. Gołaszewski, F. D'Annibale, and I. Giorgio, "A rate-independent internal friction to describe the hysteretic behavior of pantographic structures under cyclic loads," *Mechanics Research Communications*, vol. 116, p. 103761, 2021.
[58] E. Turco and E. Barchiesi, "Equilibrium paths of hencky pantographic beams in a three-point bending problem," *Mathematics and Mechanics of Complex Systems*, vol. 7, no. 4, pp. 287–310, 2019.
[59] A. Cazzani, "On the dynamics of a beam partially supported by an elastic foundation: an exact solution-set," *International Journal of structural stability and dynamics*, vol. 13, no. 08, p. 1350045, 2013.
[60] S. R. Eugster and C. Glocker, "Constraints in structural and rigid body mechanics: a frictional contact problem," *Annals of solid and structural mechanics*, vol. 5, no. 1-2, pp. 1–13, 2013.

Please cite this document as: M. Valmalle, A. Vintache, B. Smaniotto, F. Gutmann, M. Spagnuolo, A. Ciallella, F. Hild, "Local-global DVC analyses confirm theoretical predictions for deformation and damage onset in torsion of pantographic metamaterial", *Mechanics of Materials* (2022), doi:https://doi.org/10.1016/j.mechmat.2022.104379.

[61] I. Giorgio, "A discrete formulation of kirchhoff rods in large-motion dynamics," *Mathematics and Mechanics of Solids*, vol. 25, no. 5, pp. 1081–1100, 2020.

(1) ENS Paris-Saclay, DER Génie Mécanique, Gif-sur-Yvette, France

(2) Université Paris-Saclay, CentraleSupélec, ENS Paris-Saclay, CNRS, LMPS - Laboratoire de Mécanique Paris-Saclay, Gif-sur-Yvette, France

(3) Fraunhofer Institute for High-Speed Dynamics, Ernst-Mach-Institut, Freiburg, Germany

(4) Dept. of Sustainable Systems Engineering, Albert-Ludwigs-University Freiburg, Freiburg, Germany

(5) Dept. of Civil and Environmental Engineering and Architecture, University of Cagliari, Italy

(6) M&MoCS, University of L'Aquila, Italy

(7) Dept. of Civil, Construction-Architectural and Environmental Engineering, University of L'Aquila, Italy

Email address, Corresponding author (M. Spagnuolo): mario.spagnuolo@unica.it

Please cite this document as: M. Valmalle, A. Vintache, B. Smaniotto, F. Gutmann, M. Spagnuolo, A. Ciallella, F. Hild, "Local-global DVC analyses confirm theoretical predictions for deformation and damage onset in torsion of pantographic metamaterial", *Mechanics of Materials* (2022), doi:https://doi.org/10.1016/j.mechmat.2022.104379.